PAPER

Enhancing the performance of $NaNbO_3$ triboelectric nanogenerators by dielectric modulation and electronegative modification

IOP Publishing Journal of Physics D: Applied Physics
J. Phys. D: Appl. Phys. **51** (2018) 015303 (10pp) https://doi.org/10.1088/1361-6463/aa9a6c

Enhancing the performance of $NaNbO_3$ triboelectric nanogenerators by dielectric modulation and electronegative modification

Meihui Lai[1], Lu Cheng[1], Yi Xi, Yinghui Wu, Chengguo Hu, Hengyu Guo, Bolun Du, Guanlin Liu, Qipeng Liu and Ruchuan Liu

Department of Applied Physics, State Key Laboratory of Power Transmission Equipment & System Security and New Technology, Chongqing University, Chongqing 400044, People's Republic of China

E-mail: xiyi.xi@163.com (Y Xi) and phyliurc@cqu.edu.cn (R C Liu)

Received 19 October 2017
Accepted for publication 14 November 2017
Published 8 December 2017

Abstract

Increasing the triboelectric charge density on the friction layer of polydimethylsiloxane (PDMS) is a basic approach towards improving the output performance of a triboelectric nanogenerator (TENG). Most previous work focuses on the surface structure or dielectric properties, nonetheless, a few studies have focused on electronegative modification. $NaNbO_3$-PDMS TENG (N-TENG) devices are fabricated by dispersing cubic $NaNbO_3$, which is a lead-free piezoelectric material with molecular oxygen dangling bonds on the surface of the crystal, into the PDMS at different mass ratios. When the mass ratio is 7 wt%, the maximum output performance of the N-TENG is obtained. The open-circuit voltage is 550 V, the short-circuit current is 16 μA, and the effective power densities reach up to 5.5 W m^{-2} at a load resistance of ~100 MΩ. The N-TENG has been used to assemble self-powered electronic watches and illuminate commercial light-emitting diodes, respectively. Its fundamental mechanism has also been discussed in detail from the perspective of dielectric modulation and electronegative modification. This N-TENG technology is revealed to be a splendid candidate for application in large-scale device fabrication, flexible sensors and biological devices thanks to its easy fabrication process, low consumption, high output power density and biocompatibility.

Keywords: triboelectric generator (TENG), $NaNbO_3$, PDMS, dielectric permittivity, self-powered device

Supplementary material for this article is available online

(Some figures may appear in colour only in the online journal)

1. Introduction

As an attractive vision for the future, researchers have been trying to realize a real integrated micronano system, which can work continually, independently and effectively [1]. To realize this great vision, establishing a sustainable energy source is an urgent issue. A significant approach in response to this challenge for the production of sustainable green power is the harvesting of energy from our living environment [2–5]. Triboelectric nanogenerators (TENGs), which convert mechanical energy to electric energy based on the coupling of the triboelectric effect and electrostatic induction, have been proved to be an effective approach [6–10]. There are many previous studies which have investigated the structural design and surface roughness of the device, improving the output of the TENG in different ways [6, 7, 11–13].

[1] These authors contributed equally to this work.

Recently, polydimethylsiloxane (PDMS, $[Si(CH_3)_2O]_n$), which is a polymer electret, has been found to be an outstanding candidate material for TENGs [17–20], due to its attractive properties such as plasticity, transparency [14], flexibility [15] and biocompatibility [16]. Many previous studies on PDMS have been applied to TENGs, but most of them only focus on the surface structure and dielectric properties. However, electronegativity, which is an intrinsic property of triboelectric materials and critically important to the output performance of TENGs, is often ignored [21].

As we know, piezoelectric material is one of the most interesting nanomaterials that has been adopted in the area of energy harvesting because of its high dielectric permittivity and piezoelectricity [22–24]. A $NaNbO_3$ perovskite type crystal, as a lead-free piezoelectric material with a large amount of active oxygen on the surface of the crystal, has been studied in the field of piezoelectric nanogenerators (PENGs), but there have been no reports about triboelectric dielectric materials in TENGs [25]. There is some previous work that has studied TENGs for composite PDMS films, but the focus of the study was only on the dielectric properties of the composite film [26], and its electronegativity has been ignored. Therefore, it is necessary to investigate the fundamental mechanism of TENGs based on the composite PDMS film in dielectric modulation and electronegativity.

Based on the triboelectric friction of the dielectric composite film made of lead-free cubic $NaNbO_3$ and PDMS, we report a flexible, robust and cost-effective hybrid $NaNbO_3$-PDMS TENG (N-TENG), and quantitatively investigate it by modifying the PDMS with cubic $NaNbO_3$ at different mass ratios. The work frequency of the $NaNbO_3$-PDMS TENGs (N-TENGs) is 2 Hz and the periodic pressure is ~5.7 N, and this condition is suitable for daily life. Moreover, the enhancement of the output power is compared with that of pure PDMS in the same condition. Surprisingly, the highest output of the fabricated N-TENG was measured while the dispersed mass ratio was not at a maximum in this work. During the periodical compressing deformation, a stable maximum electrical signal was obtained, going up to 550 V (open-circuit voltage) and 16 μA (short-circuit current). Furthermore, an effective power density of 5.5 W m^{-2} at a load resistance of ~100 MΩ was also obtained, and has been used to assemble a self-powered electronic watch as well as illuminate 48 commercial LEDs, respectively.

Starting from the origin of the output current of the TENGs, the fundamental mechanism of the N-TENG is interpreted systematically from the perspective of dielectric modulation and electronegative modification. We proposed a qualitative analysis method based on the flat-panel capacitor structure and theoretical simulation via COMSOL software. To further investigate the electronegativity of the $NaNbO_3$-PDMS composite film of N-TENG, we designed an effective experiment to test the difference in electronegativity between the $NaNbO_3$-PDMS composite film and pure PDMS film. The result of this experiment shows that the electronegativity of the $NaNbO_3$-PDMS composite film improves. The conclusion about electronegative modification is confirmed by the difference in the potential barrier height. In short, all of the results suggest the fabricated flexible N-TENG to be an excellent candidate, which can be applied in large-scale device fabrications, flexible sensors and biological devices, because of its easy fabrication process, high output power, low consumption, satisfactory durability and biocompatibility.

2. Experimental methods

2.1. Synthesis of cubic $NaNbO_3$

Single-crystalline $NaNbO_3$ was synthesized by the hydrothermal method, 1 g Nb_2O_5 (Nb_2O_5, 99% Aladdin) powder was added to 20 ml NaOH solution, which had already been prepared with a concentration of 10 M, and then it was stirred for 30 min. The blended solution was then added to 25 ml Teflon to undergo chemical reaction at 150 °C for 6 h. After the solution had been cooled down to room temperature, the products were cleaned with ethanol and deionized water, then the products were dried in an oven at a constant temperature of 80 °C for 12 h [27]. To obtain the perovskite phase and better crystallinity, the products were subsequently annealed in air at 600 °C for 12 h.

2.2. Characterization of cubic $NaNbO_3$ samples

The morphology and crystallinity of the $NaNbO_3$ nanostructures and the composite film were analyzed by a field-emission scanning electron microscope (FE-SEM, MIRA3 TESCAN) and x-ray diffraction (XRD-6000, Shimadzu, with Cu K radiation), as shown in figures 1(a) and (b), respectively.

2.3. Fabrication of N-TENG

As for mechanical energy harvesting, a contact separation model, which is a widely used TENG fabrication technique, was employed in this work. The fabrication process has been described in figure S1 (stacks.iop.org/JPhysD/51/015303/mmedia) in the supplementary information (SI). First, to get a series of mixtures composed of cubic $NaNbO_3$ and PDMS elastomer, the synthesized cubic $NaNbO_3$ is dispersed in a PDMS elastomer at various mass ratios. Second, the mixture of cubic $NaNbO_3$ and PDMS was poured into a mold to get PDMS films of the same thickness and composite size. Then, the composite films of cubic $NaNbO_3$ mixed with PDMS (~0.6 mm thickness and $2 \times 2\,cm^2$ area) are formed after curing, as shown in figure 1(c). Finally, the prepared composite thin film is assembled in the TENG using copper (Cu) foil for the top electrode, and the $NaNbO_3$ composite PDMS film above another Cu foil for the bottom electrode. The $NaNbO_3$-PDMS TENG (N-TENG) was thus fabricated, as shown in figure 1(d). A digital image of the TENG is shown in figure 1(d), exhibiting the flexibility of the composite film.

2.4. Measurements of the TENG and composite films

A line motor (42HBS48BJ4-TR0) is utilized to drive the top and bottom electrode of the N-TENG with rhythmic periodic contact separation. The frequency of periodic contact

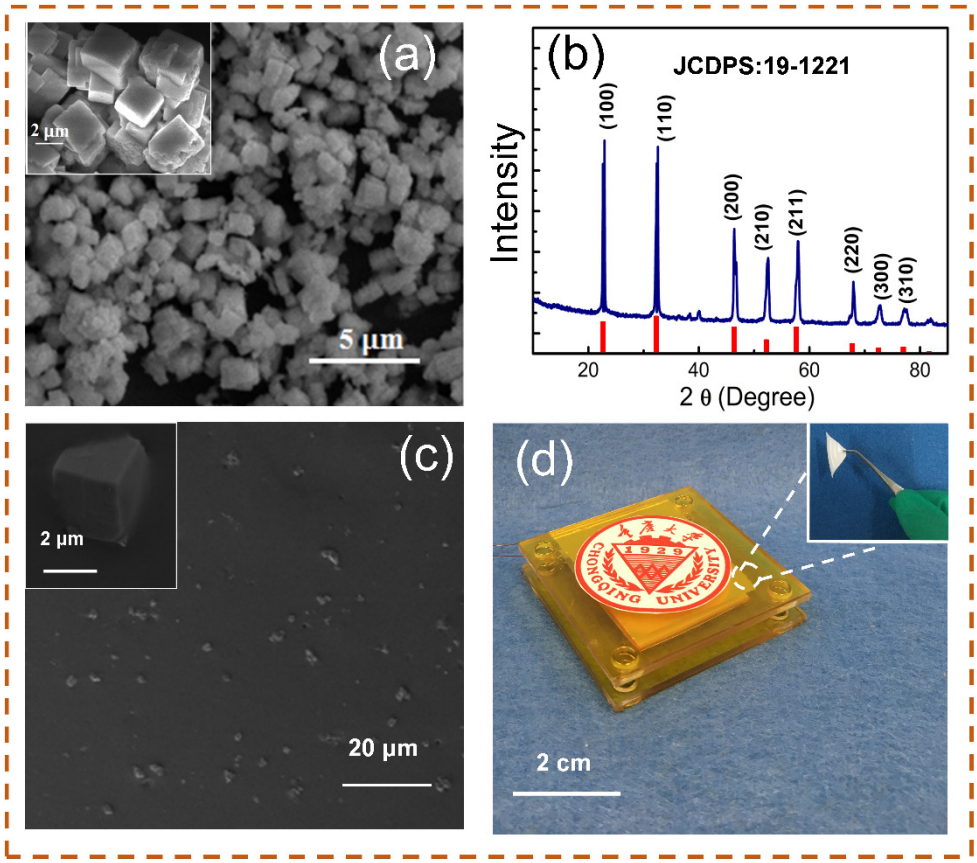

Figure 1. The FE-SEM images of (a) the hydrothermally synthesized cubic $NaNbO_3$ after the cleaning and drying steps. (b) The XRD pattern of the cubic $NaNbO_3$. (c) The surface FE-SEM images of the composite film. (d) Digital images of the TENG, with the illustration exhibiting the flexibility of the composite film.

separation is 2 Hz and the periodic pressure is ~5.7 N. The output signals generated from the N-TENG were measured by a Stanford low-noise current preamplifier (model SR570), a data acquisition card (NI PCI-6259) on a desktop PC and a Keithley 6514 system electrometer. The semiquantitative charge information of the surface of the composite film was obtained by electrostatic force microscopy (EFM), whose measurements were combined with atomic force microscopy (AFM, Asylum Research, MFP-3D) by a platinum-iridium-coated conductive probe (Nanoworld, PtIr reflex/tip coated Veeco model-SCM-PIT). The relative permittivity of the PDMS films was ascertained using a broadband dielectric spectrometer (Germany NOVOCONTROL Concept 40).

3. Results and discussion

3.1. Material characterization

The microscopic surface morphology of the hydrothermally synthesized $NaNbO_3$ is characterized by FE-SEM. The SEM images of the $NaNbO_3$ are shown in figure 1(a). It can be observed that the products are composed of cubic-shaped $NaNbO_3$ microstructures. The average particle size of these cubes is 2 μm, as shown in the inset of figure 1(a). The XRD pattern provided in figure 1(b) shows the perfect crystallinity of the $NaNbO_3$, and as a general result, it also shows that all its diffraction peaks are in accordance with those of the standard $NaNbO_3$ perovskite structures (JCPDS no. 19-1221). The FE-SEM pictures of the composite film are shown in figure 1(c), which displays how the cubic $NaNbO_3$ is well-distributed in the soft PDMS matrix.

3.2. The working mechanism of the TENG

A schematic of the N-TENG is illustrated in figure 2, with Cu foil used for the top electrode, and $NaNbO_3$-PDMS film above another copper foil for the bottom electrode. Acrylic sheets were used as insulating layers to encapsulate the TENG device. After a few cycles of pressing and releasing, thanks to the triboelectric effect and electrostatic induction, the $NaNbO_3$-PDMS film of the bottom electrode can attain a negative electron from the copper foil of the top electrode [28], and an electric charge distribution is formed, as shown in figure 2(a). When $D \gg L$, the top Cu electrode has the same quantity of positive charge as negative charge on the surface of the $NaNbO_3$-PDMS film, due to electrostatic induction. When the top electrode gets closer to the bottom electrode $D \leqslant L$, in order to keep the principle of electric neutrality, the electrons flow from the top electrode to the bottom one, resulting in an electric current from the bottom electrode to the top, as shown in figure 2(b). The positive charge in the bottom electrode will be completely neutralized by the electron flow from the top electrode, until the contact between the bottom and top electrons is complete $(D = 0)$. As shown in

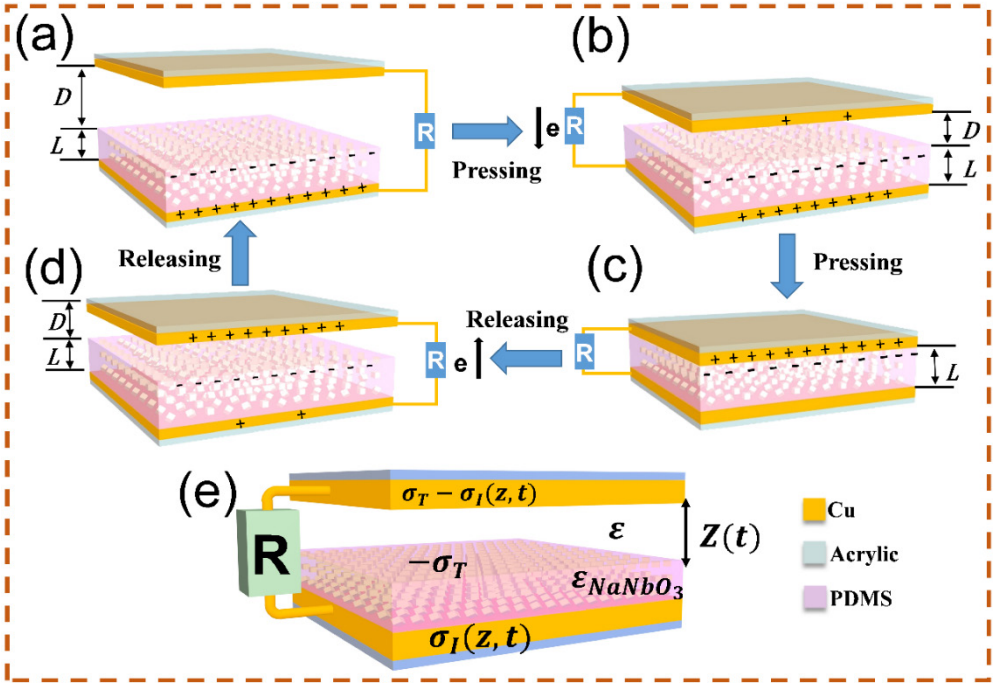

Figure 2. (a)–(d) The working mechanism of N-TENG, and a diagram of the N-TENG under a cyclic compressive force in the macrostructure. (e) The structure of the N-TENG based on a parallel capacitor.

figure 2(c), a potential difference will form between the top and bottom electrodes. Subsequently, with the top electrode leaving the bottom one, the positive charges on the top surface of the Cu electrode, which appear as electrostatic induction, decrease. The electrons flow from the bottom electrode to the top electrode, and the positive charge on the copper foil of the bottom increases, which results in an electric current from the top electrode to the bottom one in the external circuit, as shown in figure 2(d). Accordingly, with a periodic compressive force applied to N-TENG, alternative voltage and current output signals will be generated by the N-TENG.

Based on the design of the structures, we can simply take the whole N-TENG as a plane-parallel capacitor with an external load. The electron flow is driven back and forth through an external circuit in the pressing–releasing process when the N-TENG works, resulting in an alternating current (voltage) pulse being formed. From previous work, the external short-circuit current of the N-TENG is Maxwell's displacement current (I) [29], which is

$$I = J_{\mathrm{D}}S = S\frac{\partial \sigma_{\mathrm{I}}}{\partial t} = S\sigma_{\mathrm{T}}z'(t)\frac{\mathrm{d}\varepsilon_0\varepsilon}{[z(t)\varepsilon + \mathrm{d}\varepsilon_0]^2}. \quad (1)$$

As shown in figure 2(e), where J_{D} is the displacement current density of N-TENG, S is the contact area between the surface of the $NaNbO_3$-PDMS film and the top electrode, σ_{I} is the inductive charge density of the copper film of the bottom electrode, z is the distance of the gap between the dielectric ($NaNbO_3$-PDMS film) and the top electrode, σ_{T} is the triboelectric charge density of the frictional dielectric ($NaNbO_3$-PDMS film), ε is the permittivity of the $NaNbO_3$-PDMS film, d is the thickness of the $NaNbO_3$-PDMS film and ε_0 is the permittivity of the air gap. So, in certain experimental conditions (d, ε_0, and $z(t)$ are the same for different N-TENGs), the contact area between the $NaNbO_3$-PDMS film and the top electrode, the permittivity (ε) of the $NaNbO_3$-PDMS film and the triboelectric charge density (σ_{T}) of the $NaNbO_3$-PDMS film are key points, which influence the short-circuit current of N-TENGs.

3.3. The output performance of the N-TENGs

To measure the electrical signals generated by the TENG, a liner motor, a current preamplifier and a data acquisition card are used in this work. When the N-TENG is regularly deformed by a liner motor, the short-circuit current (I_{SC}) and open-circuit voltage (V_{OC}) are measured by a current preamplifier, as shown in figure 3. To further verify the output performance of the N-TENG, the I_{SC} and V_{OC} of the N-TENGs at various concentrations have been collected. The results show that the output signals increase with the $NaNbO_3$ concentration until 7 wt%, and the observed generated short-circuit current and open-circuit voltage gradually increase up to 16 μA and 550 V respectively, as shown in figures 3(a) and (b). With the further increase of the mass concentration of the cubic $NaNbO_3$, the short-circuit current of the N-TENGs decreases gradually to 5 μA at a dispersed concentration of 28 wt%, and the maximum short-circuit current is enhanced up to four times in comparison with that based on pure PDMS, as shown in figure 3(a). The charging voltage as a function of the charging time for various capacitances and the short-circuit transfer charge (Q_{sc}) of N-TENGs at various cubic $NaNbO_3$ mass ratios is also shown in figure S2 in the SI. As shown in figure 3(b), the open-circuit voltage changed with the increase of the cubic $NaNbO_3$, which reached 550 V at 7 wt%, although it decreased to 300 V, which is the same as the pure TENG film. Figures 3(c)–(e) display the load output performance of

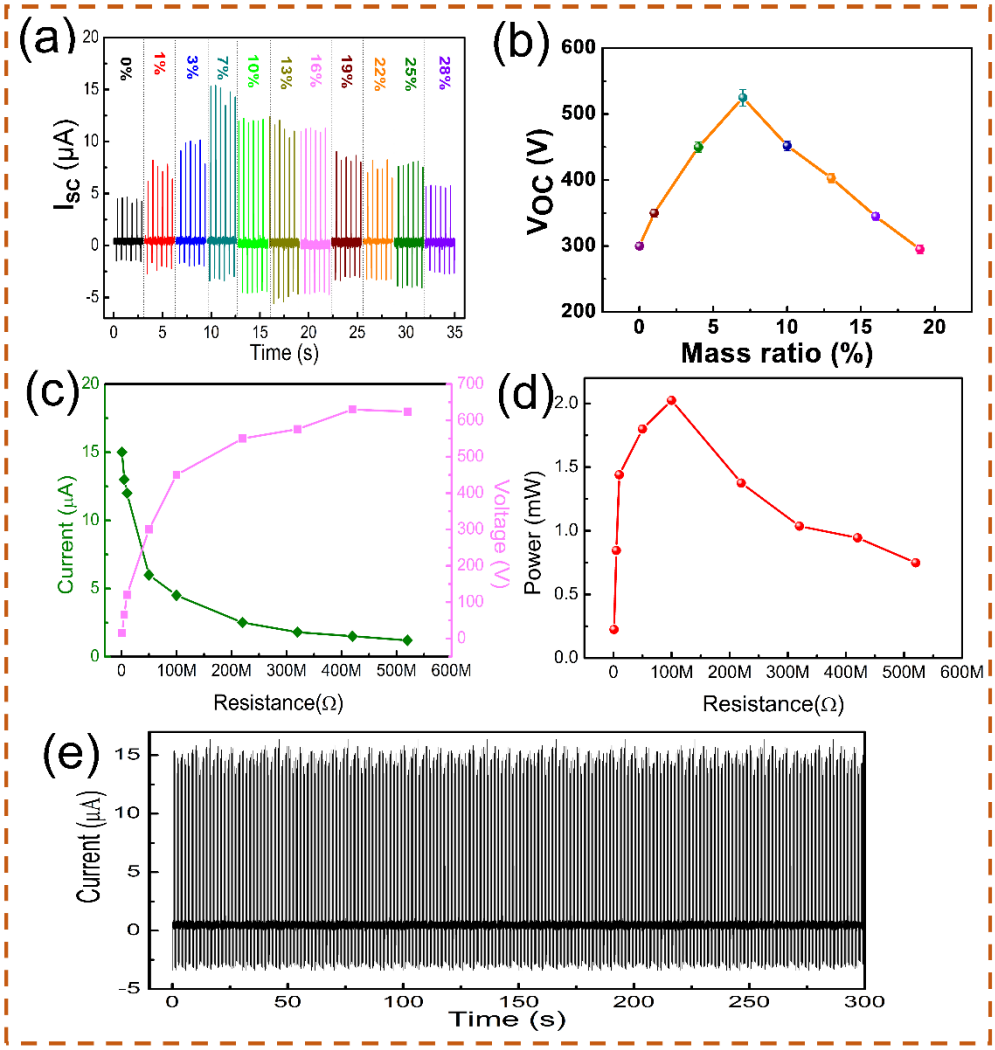

Figure 3. (a) The harvested short-circuit current (I_{SC}), and (b) the open-circuit voltage (V_{OC}) of the N-TENGs at various cubic $NaNbO_3$ mass ratios. (c) The measured voltage and current under an outer variable resistance from 0–600 MΩ. (d) The relationship between the instantaneous power outputs and load resistance, and the effective power harvested to 2.1 mW at a load resistance of 100MΩ. (e) The cycle stability of the N-TENG.

the N-TENG at 7 wt%. Figure 3(c) displays the output voltage and current as a function of load resistance from 0–600 MΩ. With the increase of the connected external resistance, the output voltage increased but the output current decreased. The instantaneous power outputs of the N-TENG were characterized by calculating the load voltage and current measured with the resistors; the maximal electrical power is about 2.2 mW at a load resistance of ~100 MΩ. The output voltage (current) as a function of load resistance and the instantaneous power output of another N-TENG with a different dispersed $NaNbO_3$ concentration are shown in figure S3 in the SI. The results show that the output power of the N-TENG at a 7 wt% dispersed $NaNbO_3$ concentration is the maximum output power. To prove its stability, the N-TENG is repeatedly compressed and released at a frequency of 2 Hz for 600 cycles (~300s). The steady output current (figure 3(e)) demonstrates the excellent stability of the N-TENG. In addition, the pressing time is extremely short—shorter than the release time—and the output current (I) can be expressed as in equation (2), leading to the pressing output current being bigger than the releasing output current, as shown in figure S4.

$$I = \frac{\mathrm{d}Q}{\mathrm{d}t}. \tag{2}$$

As we know, cubic $NaNbO_3$ perovskite, as a lead-free piezoelectric material, is not only famous for its high permittivity, but also for the oxygen molecular dangling bonds on its crystal surface. So the output performance mechanism of the N-TENGs changing with the dispersed concentration of cubic $NaNbO_3$ in the PDMS is analyzed from the point of view of these two aspects.

3.4. The influence of the high permittivity of $NaNbO_3$ for the N-TENG

As mentioned above, the high permittivity of the cubic $NaNbO_3$ perovskite in the composite PDMS TENG effects the capacitance of the TENG. From equation (1), the output current of the N-TENG is closely related to the permittivity of the composite $NaNbO_3$-PDMS film. The experimental tests of the relative permittivity of $NaNbO_3$-PDMS films with a different mass ratio are given in figure 4(a). With the increase of the dispersed mass ratio of the cubic $NaNbO_3$, the relative

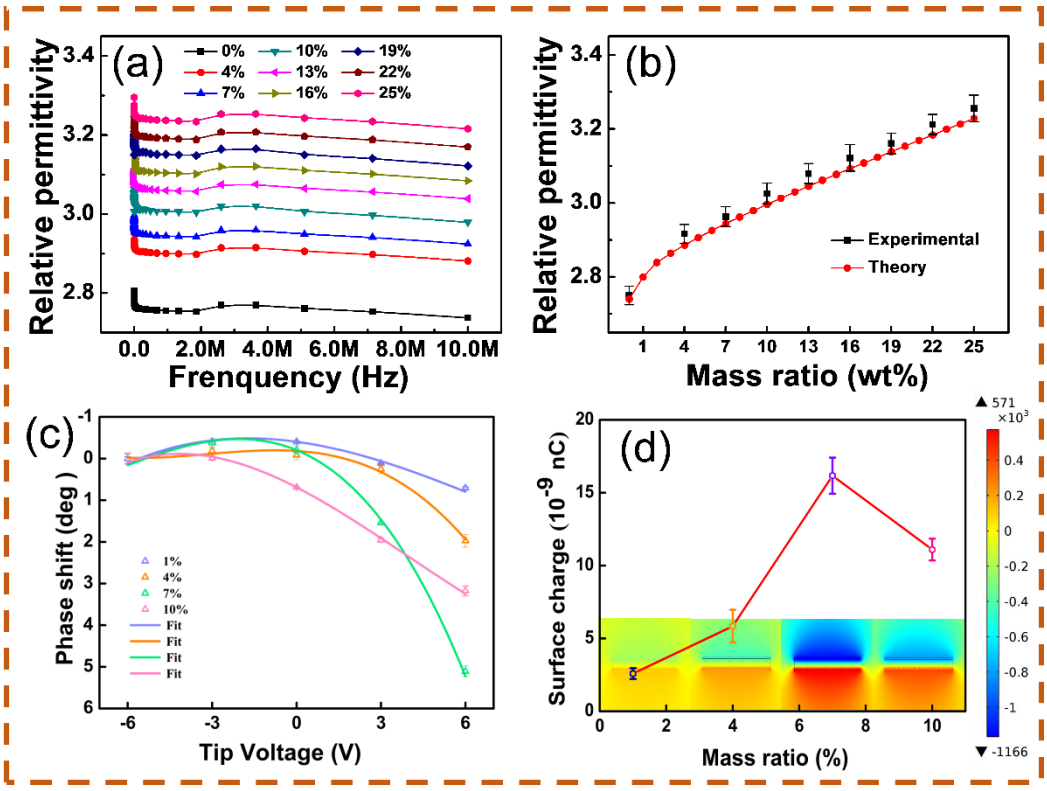

Figure 4. (a) The relative permittivity of the $NaNbO_3$ composite PDMS films. (b) The theoretical deduction of relative permittivity for the $NaNbO_3$ composite PDMS film. (c) The dependency of the surface charge measured by EFM on the composite concentration of the thin films. (d) The surface charge calculated by the EFM measurement for the composite thin film depends on the mass ratio of cubic $NaNbO_3$ dispersed in the PDMS. The insets are a potential simulation diagram of the TENGs at different mass ratios (1 wt%, 4 wt%, 7 wt% and 10 wt%).

permittivity of the composite PDMS films increases gradually. The relative permittivity of the $NaNbO_3$-PDMS films $\bar{\varepsilon}$ can be expressed theoretically

$$\bar{\varepsilon} = -\frac{\varepsilon_1\left\{\left(x^3 - x^2 + x\right)\left(\varepsilon_1 - \varepsilon_2\right) - \varepsilon_1\right\}}{\left(x^2 - x\right)\left(\varepsilon_1 - \varepsilon_2\right) + \varepsilon_1}. \tag{3}$$

The deduction of $\bar{\varepsilon}$ is presented in S5, where ε_1 is the relative permittivity of PDMS, ε_2 is the relative permittivity of $NaNbO_3$ and x is the volume ratio of $NaNbO_3$ to PDMS. As shown in figure 4(b), the theoretical results are consistent with the experimental results. In order to further study the mechanism of the output performance of the N-TENG changing with the dispersed concentration of cubic $NaNbO_3$ in the PDMS, the surface charge density of the composite film is measured by EFM. The interleaved EFM measurements were performed according to the way described by Yalcin *et al* [30]. The measured EFM data is fitted by the following polynomial equation (4),

$$\Delta\Phi = K_0 + K_1 V_{\mathrm{EFM}} + K_2 V_{\mathrm{EFM}}^2 \tag{4}$$

where $\Delta\Phi$ is the phase shift of the resonant peak (degree) [31], while K_0, K_1 and K_2 are defined as $K_1 = \frac{Q}{kz^2}q$ and $K_2 = -\frac{3Q\alpha}{kz^4}$ [32], where Q is the quality factor, k is the spring constant of the cantilever, z is the probe surface distance, q is the surface charge, α is the electric polarizability (in this study, $Q = 175$, $k = 2.8\ \mathrm{N\,m^{-1}}$ and $z = 50$ nm). Thus, from the fitting in figure 4(c), the surface charges of these films can be evaluated, as shown in figure 4(d). In figure 4(d), it is clear that the surface charge reaches a maximum at a dispersed $NaNbO_3$ concentration of 7 wt%, which is the same as the dependency of the output current/voltage on the microcube ratio in the composite $NaNbO_3$ film, as shown in figures 2(a) and (b). In addition, from the results of the EFM, we have found that with the increase of roughness, the surface charge (which is proportional to K_1) also increases (as shown in table S1). In addition, figure S6 is the FE-SEM picture of the EFM probe, which is used in this work. Whenever the sequence of measurements is 1 wt%, 4 wt%, 7 wt% and 10 wt%, we can see that the wastage in this probe is feeble, which means that the results of the measurement have almost no influence on the sequence of composite films at different dispersed mass ratios. At the same time, the triboelectric potential distributions of the composite N-TENG are calculated by a finite element analysis (FEA) method using COMSOL software. From the simulated results (the insets of figure 4(d)), with the increase of cubic $NaNbO_3$, the dispersed mass ratio of the output voltage of the TENG increases, reaching a maximum when the dispersed mass ratio is 7% and then decreasing gradually. The data from the EFM and the relative permittivity of the composite PDMS film are used in the finite element analysis. It is obvious that the simulated triboelectric potential distributions have the same variation trend as the output voltage of the TENGs, as shown in figure 4(d).

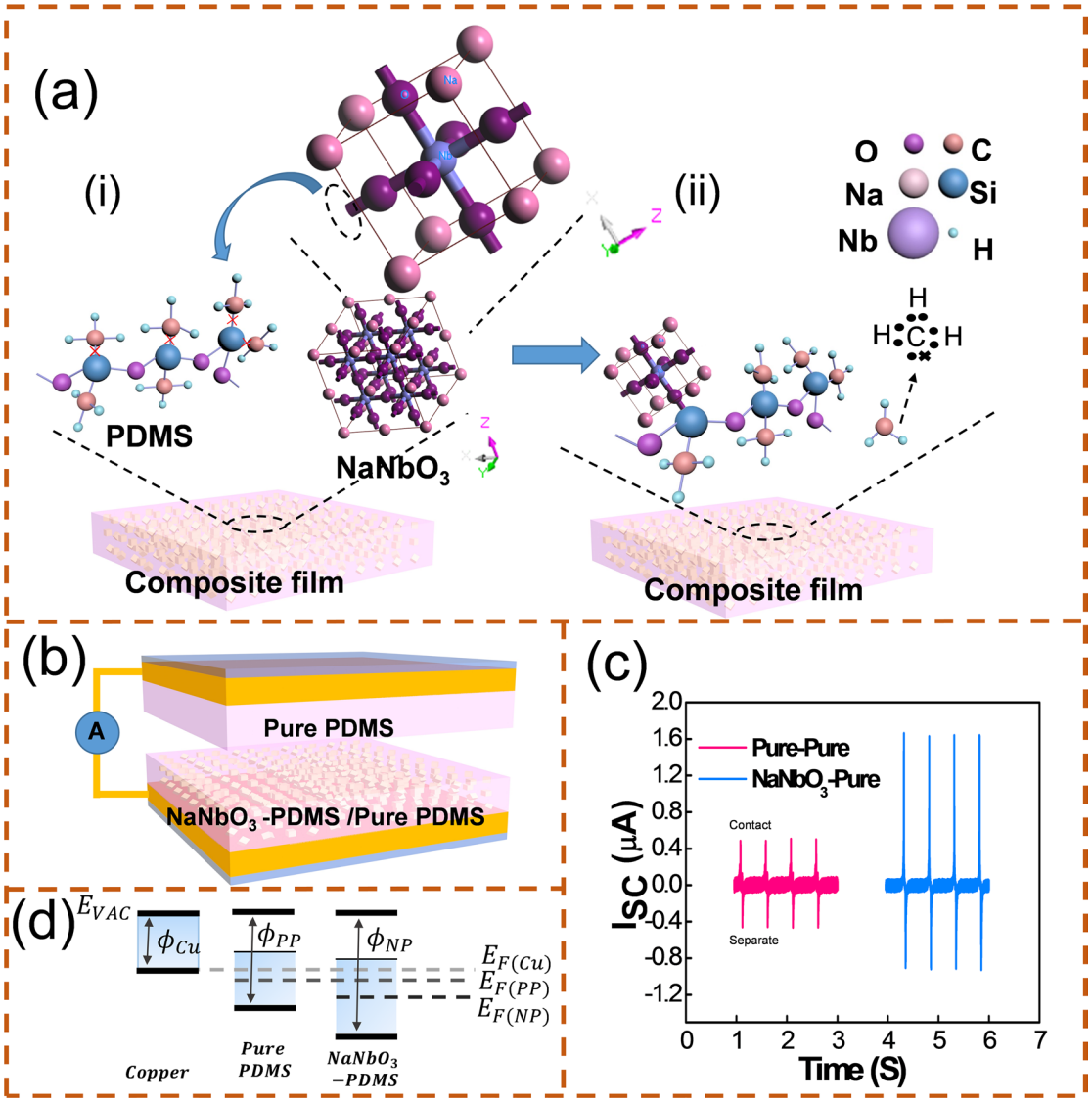

Figure 5. (a) A schematic illustration of the charge in the molecular structure of the PDMS and cubic $NaNbO_3$ based on the controlled molecular dangling bonds. (b) A cross-section of the structure of the TENGs used in the electronegativity test. (c) The short-circuit output current (I_{SC}) of the TENGs used in the electronegativity test. (d) The potential barrier of copper, pure PDMS and cubic $NaNbO_3$ composite PDMS film.

3.5. Electronegative modification

Based on the above analysis, the triboelectric charge density (σ_T) of $NaNbO_3$-PDMS film is the key point of influence on the short-circuit current (I_{SC}) of the N-TENGs. The triboelectric charge density (σ_T) on a frictional surface is decided by the difference in electronegativity between the two frictional materials [28, 33]. The molecular oxygen dangling bonds on perovskite cubic $NaNbO_3$ can increase the electronegativity of $NaNbO_3$-PDMS film to enhance the output performance of the N-TENG. With the increase of the dispersed concentration of cubic $NaNbO_3$ in the PDMS, the output performance of the TENG increases and reaches a maximum value of 550 V and 16 μA. It is the breaking of the Si–O–Si groups that results in the tribo-charge property of the composite PDMS TENG. It is well known that PDMS is extremely sensitive to free oxygen radicals, as shown in figure 5(a), and while part of the PDMS methyl group (Si-CH_3) breaks, the molecular oxygen dangling bonds on the cubic $NaNbO_3$ attack some of the broken groups (Si–O–Si–) and substitute the methyl groups (–CH_3) during the pressing process [34]. As we know, the essence of triboelectrification is that mechanical energy, which comes from the process of friction, is converted to heat energy, which stimulates the bound state of the charged particles to gain energy and go beyond the work function barrier to form a free charge. Then, these free charges are redistributed according to the potential barrier height of the frictional surface [35]. So the broken methyl groups (–CH_3) obtain free electrons (figure 5(a(ii))) produced by triboelectrification. As a result, the electronegativity of the $NaNbO_3$ composite PDMS film increases, causing the enhanced output performance of the N-TENG. In order to certify that the electronegativity of the $NaNbO_3$ composite PDMS film increases, special friction is used, as shown in figure 5(b). There are two TENGs: the normal one where both friction surfaces are pure PDMS film (pure–pure TENG), and the special TENG in which the upper friction surface is a

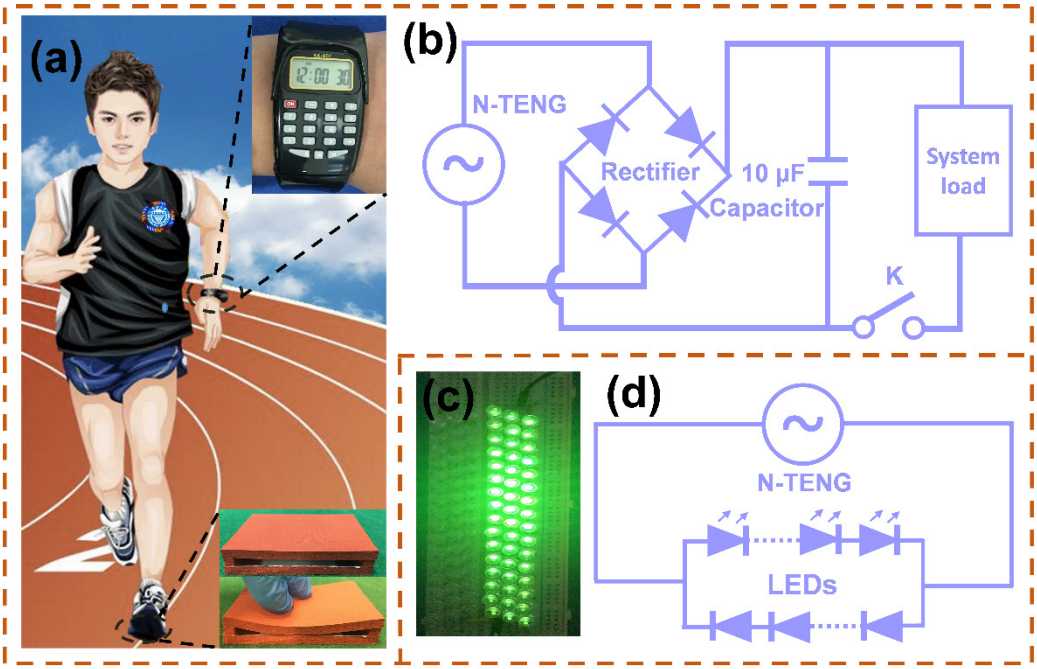

Figure 6. (a) A self-powered electronic watch used in a running scenario. (b) The charge management circuit system applied to a self-powered electronic watch. (c) The LED lighting circuit diagram. (d) Lit LEDs, which are powered directly by the TENG without using another energy source.

pure PDMS film and the bottom friction surface is a $NaNbO_3$ composite PDMS film ($NaNbO_3$–pure TENG). The output currents of the pure–pure TENG and $NaNbO_3$–pure TENG are shown in figure 5(c), and the short-circuit currents of the pure–pure TENG and $NaNbO_3$–pure TENG are 0.45 μA and 1.72 μA respectively. The output performance of the $NaNbO_3$–pure TENG is much higher than the output performance of the pure–pure TENG, which certifies that the electronegativity of the $NaNbO_3$ composite PDMS film is higher than the pure PDMS film. The difference in the electronegativity between the $NaNbO_3$ composite PDMS film and the pure PDMS film is caused by the difference of the potential barrier height of the pure PDMS film between the $NaNbO_3$ composite PDMS film (as shown in figure 5(d)). In addition, $E_{F(Cu)}$, $E_{F(PP)}$ and $E_{F(NP)}$ [36] are the Fermi level of the copper film, pure PDMS and $NaNbO_3$ composite PDMS film, respectively. The Fermi level of copper is higher than pure PDMS, which means the electrons can transfer from the copper film to pure PDMS film easily, i.e. the electronegativity of pure PDMS is stronger than copper. Similarly, the electronegativity of the $NaNbO_3$ composite PDMS film is stronger than the PDMS film.

3.6. The influence of $NaNbO_3$ on the contact area of N-TENG

Accordingly, with the increase in the amount of $NaNbO_3$, the dangling bonds increase and the surface charge density increases gradually when the $NaNbO_3$ reaches 7 wt%. However, as the mass ratio of $NaNbO_3$ grows further, the output begins to decrease. This is because the generation of triboelectric charge on the PDMS surface has already reached saturation point, which is due to the bond breaking of the Si–O–Si groups. In this case, with further increments of cubic $NaNbO_3$, more and more of it appears on the surface of the cubic $NaNbO_3$-PDMS films (figure 1(c)), causing the frictional area of the N-TENG to decrease, attenuating its output signal.

3.7. The application of the N-TENG

The N-TENG has been used in the assembly of a self-powered electronic watch, as shown in figure 6(a), which can convert the mechanical energy produced by a human to electric energy, supporting the function of the electronic watch. In addition, the charging management circuit of the self-powered electronic watch is shown in figure 6(b). With the work of the N-TENG, electric energy can also be used to light commercial LEDs without another power source (as shown in figure 6(d)). A circuit diagram of the LEDs is shown in figure 6(c), and more details can be found in videos 1 and 2 respectively.

4. Conclusion

In summary, a high-performance TENG incorporating lead-free piezoelectric cubic $NaNbO_3$ and PDMS has been reported in this work. The robust, cost-effective and biocompatible N-TENG can harvest a stable electrical output during periodical mechanical compressing and releasing states. To develop the performance of the fabricated N-TENG, we optimized a mixed mass ratio between the cubic $NaNbO_3$ and PDMS. Ultimately, it is demonstrated that a composite film with a dispersed $NaNbO_3$ mass ratio of 7 wt% can generate a maximum electrical output signal of up to 16 μA (short-circuit current), 550 V (open-circuit voltage) and a power of up to 5.5 W m^{-2} at a load resistance of ~100 MΩ, which is

four times that of the pure PDMS film TENG. The N-TENG has been used to assemble a self-powered electronic watch, and can also readily light LEDs. The fundamental mechanism of the N-TENG has also been presented, based on dielectric modulation and electronegative modification. Furthermore, the mechanism of the TENG was further confirmed by the difference of the potential barrier height. N-TENG technology reveals remarkable advantages with its easy fabrication, high performance and biocompatibility, and it is an excellent candidate for large-scale device fabrications, flexible sensors and biological devices.

Acknowledgments

This work is supported by the NSFC (51772036, 51572040 and 51402112), NSFCQ (cstc2014jcyjA50030), the Graduate Scientific Research and Innovation Foundation of Chongqing, China (Grant No. CYB17044), the Development Program ('863' Program) of China (2015AA034801), the Fundamental Research Funds for the Central Universities (CQDXWL-2014-001, CQDXWL-2013-012, 106112015CDJXY300004 and 106112017CDJXY300004), the National Key Research and Development Program, Intergovernmental International Cooperation in Science and Technology Innovation Project (Grant No. 2016YFE0111500), and the large-scale equipment sharing fund of Chongqing University.

ORCID iDs

Yi Xi https://orcid.org/0000-0002-7559-8364

References

[1] Wang Z L 2013 Triboelectric nanogenerators as new energy technology for self-powered systems and as active mechanical and chemical sensors *ACS Nano* **7** 9533–57
[2] Bai P, Zhu G, Lin Z-H, Jing Q, Chen J, Zhang G, Ma J and Wang Z L 2013 Integrated multi layered triboelectric nanogenerator for harvesting biomechanical energy from human motions *ACS Nano* **7** 3713–9
[3] Yang Y, Zhu G, Zhang H, Chen J, Zhong X, Lin Z-H, Su Y, Bai P, Wen X and Wang Z L 2013 Triboelectric nanogenerator for harvesting wind energy and as self-powered wind vector sensor system *ACS Nano* **7** 9461–8
[4] Guo H, He X, Zhong J, Zhong Q, Leng Q, Hu C, Chen J, Tian L, Xi Y and Zhou J 2014 A nanogenerator for harvesting airflow energy and light energy *J. Mater. Chem.* A **2** 2079–87
[5] Chun J, Kim J W, Jung W-S, Kang C-Y, Kim S-W, Wang Z L and Baik J M 2015 Mesoporous pores impregnated with Au nanoparticles as effective dielectrics for enhancing triboelectric nanogenerator performance in harsh environments *Energy Environ. Sci.* **8** 3006–12
[6] Huang L B, Bai G, Wong M C, Yang Z, Xu W and Hao J 2016 Magnetic-assisted noncontact triboelectric nanogenerator converting mechanical energy into electricity and light emissions *Adv. Mater.* **28** 2744–51
[7] Yu A *et al* 2016 Triboelectric nanogenerator as a self-powered communication unit for processing and transmitting information *ACS Nano* **10** 3944–50
[8] Luo J, Fan F R, Jiang T, Wang Z, Tang W, Zhang C, Liu M, Cao G and Wang Z L 2015 Integration of micro-supercapacitors with triboelectric nanogenerators for a flexible self-charging power unit *Nano Res.* **8** 3934–43
[9] Zhu G, Lin Z-H, Jing Q, Bai P, Pan C, Yang Y, Zhou Y and Wang Z L 2013 Toward large-scale energy harvesting by a nanoparticle-enhanced triboelectric nanogenerator *Nano Lett.* **13** 847–53
[10] Saravanakumar B, Soyoon S and Kim S-J 2014 Self-powered pH sensor based on a flexible organic-inorganic hybrid composite nanogenerator *ACS Appl. Mater. Interfaces* **6** 13716–23
[11] Kwon Y H, Shin S-H, Jung J-Y and Nah J 2016 Scalable and enhanced triboelectric output power generation by surface functionalized nanoimprint patterns *Nanotechnology* **27** 205401
[12] Xia X, Liu G, Guo H, Leng Q, Hu C and Xi Y 2015 Honeycomb-like three electrodes based triboelectric generator for harvesting energy in full space and as a self-powered vibration alertor *Nano Energy* **15** 766–75
[13] Li X H, Han C B, Jiang T, Zhang C and Wang Z L 2016 A ball-bearing structured triboelectric nanogenerator for nondestructive damage and rotating speed measurement *Nanotechnology* **27** 085401
[14] Zhang M *et al* 2015 A hybrid fibers based wearable fabric piezoelectric nanogenerator for energy harvesting application *Nano Energy* **13** 298–305
[15] Fan F R, Tang W and Wang Z L 2016 Flexible nanogenerators for energy harvesting and self-powered electronics *Adv. Mater.* **28** 4283–305
[16] Yue X L, Xi Y, Hu C U, He X M, Dai S G, Cheng L and Wang G 2015 Enhanced output-power of nanogenerator by modifying PDMS film with lateral ZnO nanotubes and Ag nanowires *RSC Adv.* **5** 32566–71
[17] Deng W, Zhang B, Jin L, Chen Y, Chu W, Zhang H, Zhu M and Yang W 2017 Enhanced performance of ZnO microballoon arrays for a triboelectric nanogenerator *Nanotechnology* **28** 135401
[18] Wang G, Xi Y, Xuan H, Liu R, Chen X and Cheng L 2015 Hybrid nanogenerators based on triboelectrification of a dielectric composite made of lead-free $ZnSnO_3$ nanocubes *Nano Energy* **18** 28–36
[19] Kim K N, Jung Y K, Chun J, Ye B U, Gu M, Seo E, Kim S, Kim S-W, Kim B-S and Baik J M 2016 Surface dipole enhanced instantaneous charge pair generation in triboelectric nanogenerator *Nano Energy* **26** 360–70
[20] Zhang X-S, Han M-D, Wang R-X, Zhu F-Y, Li Z-H, Wang W and Zhang H-X 2013 Frequency-multiplication high-output triboelectric nanogenerator for sustainably powering biomedical microsystems *Nano Lett.* **13** 1168–72
[21] Chen J, Guo H, He X, Liu G, Xi Y, Shi H and Hu C 2016 Enhancing performance of triboelectric nanogenerator by filling high dielectric nanoparticles into sponge PDMS film *ACS Appl. Mater. Interfaces* **8** 736–44
[22] Ali D, Yu B, Duan X, Yu H and Zhu M 2017 Enhancement of output performance through post-poling technique on $BaTiO_3$/PDMS-based triboelectric nanogenerator *Nanotechnology* **28** 075203
[23] Lin Z H, Yang Y, Wu J M, Liu Y, Zhang F and Wang Z L 2012 $BaTiO_3$ Nanotubes-based flexible and transparent nanogenerators *J. Phys. Chem. Lett.* **3** 3599–604
[24] Jung J H, Chen C-Y, Yun B K, Lee N, Zhou Y, Jo W, Chou L-J and Wang Z L 2012 Lead-free $KNbO_3$ ferroelectric nanorod based flexible nanogenerators and capacitors *Nanotechnology* **23** 375401

[25] Jung J H, Lee M, Hong J-I, Ding Y, Chen C-Y, Chou L-J and Wang Z L 2011 Lead-free $NaNbO_3$ nanowires for a high output piezoelectric nanogenerator *ACS Nano* **5** 10041–6
[26] He X, Guo H, Yue X, Gao J, Xia Y and Hu C 2015 Improving energy conversion efficiency for triboelectric nanogenerator with capacitor structure by maximizing surface charge density *Nanoscale* **7** 1896–903
[27] Zhu H Y *et al* 2006 Structural evolution in a hydrothermal reaction between Nb_2O_5 and NaOH solution: from Nb_2O_5 grains to microporous $Na_2Nb_2O_6$ center dot(2)/$3H_2O$ fibers and $NaNbO_3$ cubes *J. Am. Chem. Soc.* **128** 2373–84
[28] Lacks D J and Sankaran R M 2011 Contact electrification of insulating materials *J. Phys. D: Appl. Phys.* **44** 453001
[29] Wang Z L 2017 On Maxwell's displacement current for energy and sensors: the origin of nanogenerators *Mater. Today* **20** 74–82
[30] Yalcin S E, Labastide J A, Sowle D L and Barnes M D 2011 Spectral properties of multiply charged semiconductor quantum dots *Nano Lett.* **11** 4425–30
[31] Heim T, Lmimouni K and Vuillaume D 2004 Ambipolar charge injection and transport in a single pentacene monolayer island *Nano Lett.* **4** 2145–50
[32] Kim J, Jasper W J and Hinestroza J P 2006 Charge characterization of an electrically charged fiber via electrostatic force microscopy *J. Eng. Fibers Fabrics* **1** 30–46
[33] Duke C B and Fabish T J 1978 Contact electrification of polymers—quantitative model *J. Appl. Phys.* **49** 315–21
[34] Fan F R, Luo J, Tang W, Li C, Zhang C, Tian Z and Wang Z L 2014 Highly transparent and flexible triboelectric nanogenerators: performance improvements and fundamental mechanisms *J. Mater. Chem.* A **2** 13219–25
[35] Chang Y-P, Chiou Y-C and Lee R-T 2008 Tribo-electrification mechanisms for dissimilar metal pairs in dry severe wear process—Part I. Effect of speed *Wear* **264** 1085–94
[36] Seung W *et al* 2017 Boosting power-generating performance of triboelectric nanogenerators via artificial control of ferroelectric polarization and dielectric properties *Adv. Energy Mater.* **7** 1600988